Supplementary Methods

Identification and selection of planarian ECM genes

To identify and select planarian ECM components for assessment with stem cell regulatory functions, homologs mammalian ECM genes are used, with the notion that the information gained will be more relevant and translate to mammalian stem cell function. The publicly available human and mouse matrisome database (1) (http://matrisomeproject.mit.edu/) is used to build a candidate gene list. ECM genes in the matrisome database are categorized into core ECM (involved in structural organization), ECM-affiliated (secreted proteins interacting with core ECM), ECM regulators (enzymes that modify ECM), and ECM receptors (membrane proteins that interact with ECM). From the matrisome database, a set of candidate genes is identified that included all core ECM (186 genes), ECM-related proteins that physically interact with core ECM (38 genes), and a subset of ECM-affiliated and regulator genes shown to have roles to modify or degrade core ECM and related proteins (72 genes).

The peptide sequences of the identified ECM and related genes were extracted from NCBI human protein database and searched using protein BLAST against the online available *S. mediterranea* genomic databases (PlanMine: http://planmine.mpi-cbg.de/planmine/begin.do and SmedGD: http://smedgd.stowers.org/) that resulted in the identification of 217 potentially related planarian genes, all with e-value <0.01. As a validation of matrisome/ECM identity, these planarian genes were assessed from a reverse-BLAST against the human and *C. elegans* protein databases (NCBI-nr), matching peptide domains with closest homology with a human/*C. elegans* ECM, and with a criteria that the sequence should contain least one ECM-related domain as predicted by the simple modular architecture research tool (SMART) (SI Appendix, Fig. S1*A*).

This selection protocol identified 165 candidates with ECM or ECM-related function/characteristic. This set represents our primary list of high confidence as ECM genes for functional assessing (Fig. 1*A*). The remaining 68 candidates will serve as secondary list of reference genes for future assessment or in data interpretation as they contain ECM-related domains but share closest homology with a non-ECM related protein in human and *C. elegans* genome.

Phylogenetic analysis of planarian collagens

Sequences for phylogenetic analysis were obtained from representative species as summarised in (SI Appendix, Dataset S2) and aligned using the NC1 domain for Type IV collagens, and the triple helical domain and NC1 domain for fibrillar collagens. Alignments were carried out on EBI using the MUSCLE multiple sequence alignment program (2), and gaps were removed using Gblocks (3). Maximum likelihood phylogenetic trees under different models (Dayhoff, JTT, LG, LG4X, LG4M, VT, WAG) were built using the IQ-TREE web server (4), and the best fitting model was selected for the final tree. LG4X was selected for Type IV collagen and fibrillar collagen NC1 domain alignments. VT+R3 was selected for fibrillar collagen triple helix alignments. Trees were assessed for reliability using 10,000 ultra-fast bootstrap replicates (5).

Planarian maintenance, γ-irradiation and RNAi

Asexual *Schmidtea mediterranea* strain CIW4 were kept as previously described (6). For neoblast repopulation assay, planarians were irradiated by a sub-lethal dose of 1,250 rad of γ-irradiation from a ^{137}Cs source (7). For experiments where all neoblasts from the body needed to be removed, worms were exposed to a lethal dose of 6,000 rad of γ-irradiation. For RNAi experiments, cDNAs of candidate genes were cloned into a pPR-T4P vector as previously described (8), transformed into HT115 bacteria. Preparation of bacterial RNAi food were performed as previously described (9). Briefly, transformed bacteria were grown in 100 ml of 25 μg/ml Kanamycin-supplemented 2xYT medium, 37°C with shaking, to an O.D.600 of 0.8, followed by induction with 1 mM IPTG for 2 hours. Cultured bacteria were centrifuged in 3,000 g for 8 min. Pallet was mixed with 500 μl of liver paste (1/200th of the total culture volume) and food dye by vortexing and pipetting, aliquoted and kept as stocks in -80°C. Liver paste is made in a 3:1 ratio between liver and planarian water. For a negative *control(RNAi)*, *GFP* was used as the gene to generate dsRNA as previously described (10). To initiate the experiments, worms were starved for one week, and then fed with RNAi food once every 3 days for 8 doses unless otherwise specified. After each feeding, worms are examined, where those did not uptake the RNAi food are removed from the experiments. Amputation or γ-irradiation was performed 7 days after the last RNAi feed. Gene knock down efficiency across different groups was assessed by qRT-PCR (SI Appendix, Fig. S15*G*).

In worms where RNAi of two genes (double RNAi) are to be performed. In such experiments, all RNAi groups were fed with same amount of total bacterial dsRNA food. Thus, single gene RNAi worms in such a group of experiments were fed with equal amount of control (*GFP*) RNAi food, balancing the dosage to that in double RNAi worms.

Quantitative real-time PCR

cDNA samples for qRT-PCR were synthesized by reverse transcription reaction from total RNA extracted from approximately 3 - 10 worms using a SuperScript III Reverse Transcriptase Kit (Invitrogen) or PrimeScript RT Reagent Kit with gDNA Eraser (Takara). To confirm complete removal of genomic DNA, negative controls were done where the RNA samples underwent RT but without reverse transcriptase added, PCR is done on these samples using *gapdh* qPCR primers, to check if amplification of genomic DNA occurred. Reactions were performed in technical triplicate and biological triplicate on a Bio-Rad CFX96 Touch Real-Time PCR Detection System with SYBR Green PCR Master Mix (Roche) as per manufacturer's instructions. For the amplification of each gene, primers were designed to enclose between 80 – 200 bp. For each reaction, around 10 ng of cDNA template and 0.6 µM of each primer were used; annealing temperature was set to be 60°C followed by 20 s of elongation. Relative expression levels of analyzed gene were determined by normalizing the C_T value ($2^{CT(gapdh)-CT(gene)}$) with the house-keeping gene, *gapdh* (11).

Single cell transcriptomic data analysis

A single cell transcriptomic dataset were collected from previously published study (12). tSNE plots of all genes mentioned in this study can be found in publicly available Reddien group's Digiworm website (https://digiworm.wi.mit.edu/). Data obtained for gene expression violin plots are obtained from GEO accession: GSE111764.

Whole mount ISH and antibody staining

Whole mount ISH and FISH were performed as previously described (9, 13). Samples for COLIV immunostaining were killed in 2% HCl and fixed in Methacarn (6:3:1 Methanol: Chloroform: Acetic acid) for 30 minutes on a roller at 4°C, before bleaching overnight in 6% H2O2 in methanol. Riboprobes were prepared with digoxygenin (DIG), fluorescein (FITC), or dinitrophenyl (DNP) labelling mix. Blocking buffer was prepared with 5% (v/v) horse serum, 0.5%

(v/v) Roche Western Blocking Reagent, in MABT (100mM maleic acid, 150mM NaCl, 0.1% Tween-20, pH 7.5). Anti-riboprobe antibodies used include anti-DIG-AP (1:4000), anti-DIG-POD (1:500), anti-FITC-POD (1:300), or anti-DNP-AP (1:2000). Colorimetric stains were developed using 4-nitro blue tetrazolium chloride (NBT, Roche 11383213001) with 5-bromo-4-chloro-3-indolyl-phosphate (BCIP, Roche 11383221001). FISH stains were developed with either tyramide amplification, or Fast Blue B Salt (Sigma D9805) with naphthol AS-MX phosphate (Sigma 855). Tyramide amplifications were performed in 0.1M borate buffer, pH 8.5(14). DAPI (Sigma, D9542) is added together with mounting medium to counterstain brain, VNC and intestinal structures. Intestinal boundary outlined in Fig. 6 *A, B* and *E* is determined by DAPI signal which can be visualized under higher brightness and contrast than the presented images.

For immunostainings, antibodies were used to detect phospho-histone H3 (rabbit monoclonal anti-H3ser10p, 1:1,000, Millipore 05-817R-I), COLIV (rabbit polyclonal anti-collagen IV, 1:400, Abcam ab6586) (15) and muscle (mouse monoclonal anti-6G10, 1:1,000, Hybridoma Bank 6G10-2C7, deposited to the DSHB by Zayas, R.M). Secondary horseradish peroxidase (HRP)-conjugated anti-mouse or anti-rabbit antibodies (Jackson Immunoresearch 115-036-006 and 111-035-144) was used at 1:500, with subsequent tyramide amplification. Confocal images were taken from these FISH/IF-stained samples, on either Carl Zeiss LSM700 laser scanning confocal microscope, or Leica DMIRE2 inverted fluorescence microscope with a Hamamatsu Back-Thinned EM-CCD camera and spinning disc confocal scan head. For whole animal or broad-range images, tiled images were combined by stitching, with 10% overlap between neighboring tiles. For Z-stacking, thickness between neighboring Z-sections is 5 or 10 μm. Raw confocal images were processed in Fiji image-J, Adobe Photoshop. Figures were assembled in Inkscape. Colorimetric ISH were imaged on a Leica M165 fluorescent dissecting microscope.

TUNEL and BrdU pulse-chase experiment

TUNEL staining and BrdU pulse-chase experiments are performed as previously described (9). For TUNEL staining, Terminal Deoxynucleotidyl Transferase (TdT) enzyme (Thermo, EP0162) is used. Worms used for this assay are pre-fixed and dehydrated in 100% ethanol for less than 3 days. Worms were bleached in 6% H_2O_2 diluted in PBSTx under direct light before

staining. During staining, less than 10 worms were immersed in 40µl of labeling mix (28µl reaction buffer, 12µl TdT enzyme mix) at 37°C for 2 hours. This process was repeated once, before proceeded to MABT wash, 1 hour Roche Western blocking and overnight 1:1000 anti-DIG-POD staining. For BrdU pulse-chase experiments, BrdU (Sigma B5002-5G, 25 mg/ml) was dissolved in 50% ethanol to became a 10x stock (100 mg/ml), which was further diluted into liver paste in 1:9 ratio with food dye immediately before fed to animals (9). For BrdU detection, worms were harvested 4 day-post-feeding and stained as previously described (9) with anti-BrdU antibody (BD #347580, 1:300 in blocking solution). For BrdU staining combined with FISH, acid hydrolyzation and antibody labeling steps were performed after FISH staining procedure.

Neoblast culturing on planarian decellularized matrix scaffold

RNAi worms of size less than 3mm length were harvested by rinsing in 5% NAC on the 7th day post-8 RNAi feeds (8fd7) for scaffold extraction, then rinsing in H_2O and freeze-thaw in -30°C. Epidermis is removed by forceps, followed by 1% TritonX100 (in H_2O) wash in room temperature for 2 hours in a petri dish with nutation, followed by H_2O for 5 times, 5 min each, then DNase I in DNase buffer (Invitrogen, #18068015) for 2 hours in 37 °C. Lastly, washed by PBS 5 times, 5 min per wash, and transferred into an Eppendorf tube with 500µl of IPM medium. For neoblast preparation, wild type worms of 5mm length were first pre-incubated at least one overnight in planarian water with 50µg/ml of neomycin sulfate. Worms were rinsed twice by cold CMF solution, and gently grounded up by a sterile plastic pestle in a 1.5ml Eppendorf tube. Cell/CMF mixture was passed through a 20 µm filter, followed by a 10µm filter to remove most large size cells (neoblasts have diameter less than 10µm), then centrifuged in 300 g for 5 min. Supernatant was removed and pallet was resuspended by Isotonic Planarian Medium (IPM) (16-18) with antibiotics (penicillin and streptomycin) and 1% FBS. Cells from 5 worms are suspended in 1 ml of IPM. For neoblast-ECM incubation, 500µl of cells were added into the Eppendorf tubes that already contained 500µl of IPM with ECM scaffold, then centrifuged at 300g for 5min to facilitate seeding. Mixture was cultured in dark, room temperature. IPM solution was replaced every day during incubation. To harvest for FISH staining, culture was incubated with 4% formaldehyde (in PBS) for 10min, followed by PBS rinse and then brought to perform FISH staining with same protocol as described above. One liter of IPM contains Hepes (free acid) 7208.8mg, Hepes (sodium salt) 3514.1mg, NaCl 985.4mg, $NaHCO_3$ 800.1mg, KCl 26.4mg, $CaCl_2$ 113.23mg, $MgSO_4$ 44.02mg, $MnCl_2$ 0.19mg,

$KH2PO_4$ 68.5mg, d-biotin 0.3mg, D-glucose 300.0mg, D-trehalose 50.0mg, tricine 2.5mg, MEM essential amino acids solution 2ml, MEM non-essential amino acids solution 5.00ml, MEM vitamin solution 3ml, Sodium pyruvate (100x) 14ml, 100x Pen/Strep 10ml, L-glutamine (100x) 2ml, and 1% FBS. pH was adjusted to 7.3.

Transmission electron microscopy

Preparation of samples and imaging procedures are done as described previously (9). Sample preparation and imaging were done at the Nanoscale Imaging Facility at the Hospital for Sick Children.

Statistical quantifications

Densities of different cell types and co-localizations were determined by cell number quantification using the “cell counter” function or “Threshold” and then “analyze particle” functions in the software Fiji ImageJ (available at: http://rsb.info.nih.gov/ij/). Signal intensity of images are quantified by Grey value, where all images within the same experiment were taken under the same microscope settings and processing. When cell densities, tissue length/area or gene expression levels were compared between experimental and control groups, Student two-tailed t-test assuming unequal variance was applied to determine any statistical significance, which is stated in the figure legends, together with number of animals in each group (N value). All statistical testing on data were performed with Excel. All graphs were plotted with GraphPad Prism v8.0. For dot plots, each point represents a single measurement; For bar graphs, each bar shows the mean value; each error bar represents Standard Error of the Mean (s.e.m).

Data availability

The authors declare that all data supporting the findings of this study are available within the article and its Supplementary Information files or from the corresponding author upon reasonable request.

References

1. R. O. Hynes, A. Naba, Overview of the matrisome--an inventory of extracellular matrix constituents and functions. *Cold Spring Harb Perspect Biol* **4**, a004903 (2012).
2. F. Madeira *et al.*, The EMBL-EBI search and sequence analysis tools APIs in 2019. *Nucleic Acids Res* **47**, W636-W641 (2019).
3. J. Castresana, Selection of conserved blocks from multiple alignments for their use in phylogenetic analysis. *Mol Biol Evol* **17**, 540-552 (2000).
4. J. Trifinopoulos, L. T. Nguyen, A. von Haeseler, B. Q. Minh, W-IQ-TREE: a fast online phylogenetic tool for maximum likelihood analysis. *Nucleic Acids Res* **44**, W232-235 (2016).
5. D. T. Hoang, O. Chernomor, A. von Haeseler, B. Q. Minh, L. S. Vinh, UFBoot2: Improving the Ultrafast Bootstrap Approximation. *Mol Biol Evol* **35**, 518-522 (2018).
6. A. Sanchez Alvarado, P. A. Newmark, S. M. Robb, R. Juste, The Schmidtea mediterranea database as a molecular resource for studying platyhelminthes, stem cells and regeneration. *Development (Cambridge, England)* **129**, 5659-5665 (2002).
7. B. J. Pearson, A. Sanchez Alvarado, A planarian p53 homolog regulates proliferation and self-renewal in adult stem cell lineages. *Development (Cambridge, England)* **137**, 213-221 (2010).
8. P. A. Newmark, P. W. Reddien, F. Cebria, A. Sanchez Alvarado, Ingestion of bacterially expressed double-stranded RNA inhibits gene expression in planarians. *Proc Natl Acad Sci U S A* **100 Suppl 1**, 11861-11865 (2003).
9. N. Lindsay-Mosher, A. Chan, B. J. Pearson, Planarian EGF repeat-containing genes megf6 and hemicentin are required to restrict the stem cell compartment. *PLoS Genet* **16**, e1008613 (2020).
10. M. W. Cowles *et al.*, Genome-wide analysis of the bHLH gene family in planarians identifies factors required for adult neurogenesis and neuronal regeneration. *Development (Cambridge, England)* **140**, 4691-4702 (2013).
11. G. T. Eisenhoffer, H. Kang, A. Sanchez Alvarado, Molecular analysis of stem cells and their descendants during cell turnover and regeneration in the planarian Schmidtea mediterranea. *Cell Stem Cell* **3**, 327-339 (2008).
12. C. T. Fincher, O. Wurtzel, T. de Hoog, K. M. Kravarik, P. W. Reddien, Cell type transcriptome atlas for the planarian Schmidtea mediterranea. *Science* **360** (2018).
13. B. J. Pearson *et al.*, Formaldehyde-based whole-mount in situ hybridization method for planarians. *Dev Dyn* **238**, 443-450 (2009).

14. A. A. Raz, M. Srivastava, R. Salvamoser, P. W. Reddien, Acoel regeneration mechanisms indicate an ancient role for muscle in regenerative patterning. *Nat Commun* **8**, 1260 (2017).
15. D. Bansal *et al.*, Cytoplasmic poly (A)-binding protein critically regulates epidermal maintenance and turnover in the planarian Schmidtea mediterranea. *Development (Cambridge, England)* **144**, 3066-3079 (2017).
16. W. P. Schürmann, R. , Planarian cell culture: a comparative review of methods and an improved protocol for primary cultures of neoblasts. *Belg. J. Zool* **123-130** (2001).
17. W. T. Teshirogi, K., Primary tissue culture of freshwater planarian in a newly devised medium. *Fortschr. Zool.* **36**, 91-96 (1988).
18. K. Lei, S. A. McKinney, E. J. Ross, H.-C. Lee, A. S. Alvarado, Cultured pluripotent planarian stem cells retain potency and express proteins from exogenously introduced mRNAs. *bioRxiv* 10.1101/573725, 573725 (2019).

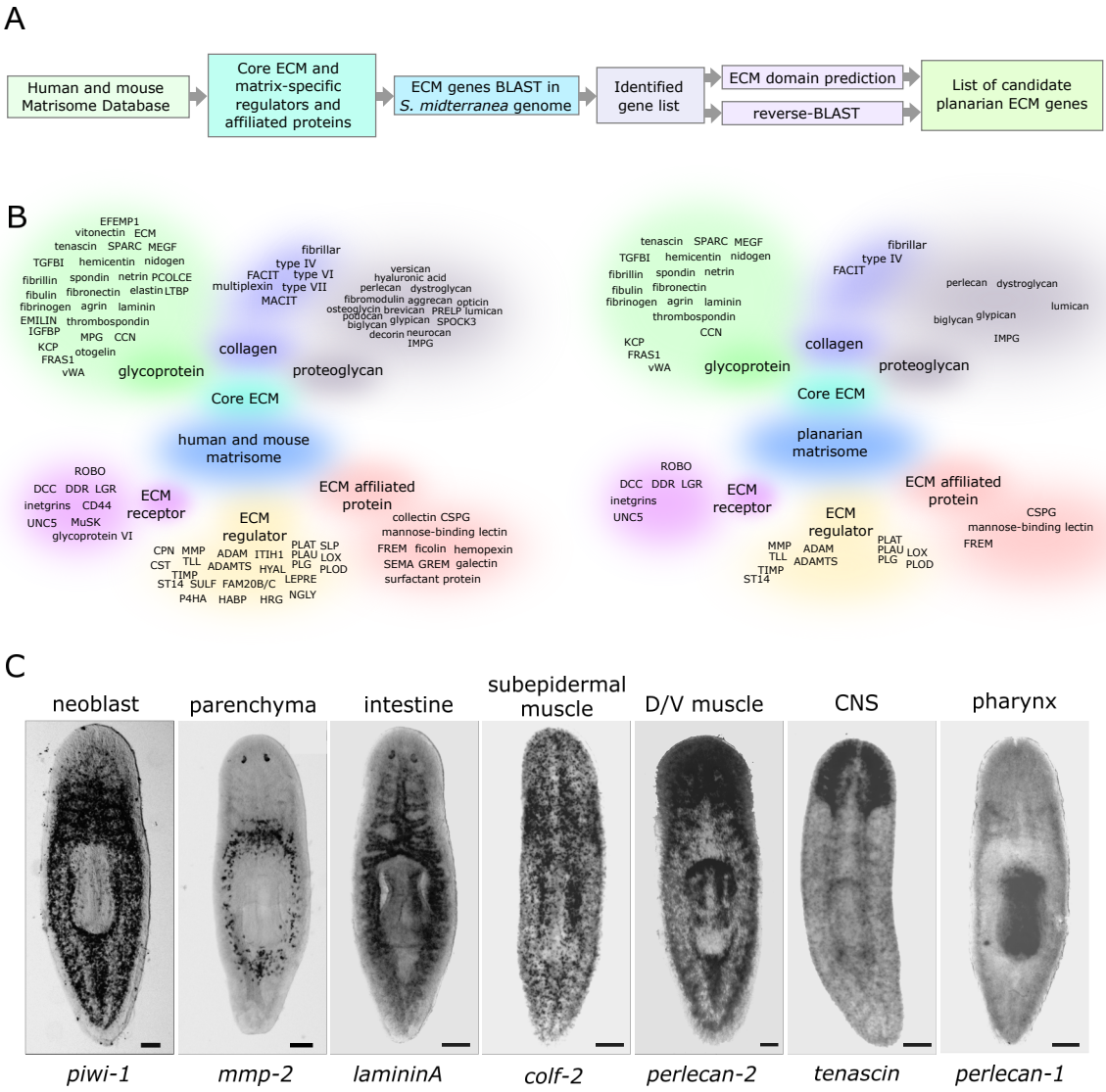

Figure S1. Identification of ECM in planarian.
(*A*) Outline of planarian ECM candidate gene identification and selection from the human and mouse matrisome database, and the planarian genomic database. (*B*) Summary of ECM in human and mouse matrisome (Right), and ECM identified in *S. mediterranea* genome (Left). ECM genes are grouped according to their corresponding families, including core ECM, ECM receptor, regulator and affiliated proteins. (*C*) Whole mount colorimetric-ISH showing neoblast (*piwi-1*) localization, as compared to ECM genes expressed in D/V muscles (perlecan-2), gut (laminin-A), subepidermal muscles (colf-2) and parenchymal cells (mmp-2), stained by ISH. These ECM-expressing tissues have different degree of proximity to the neoblast compartment (*piwi-1*). Scale bar = 100 μm.

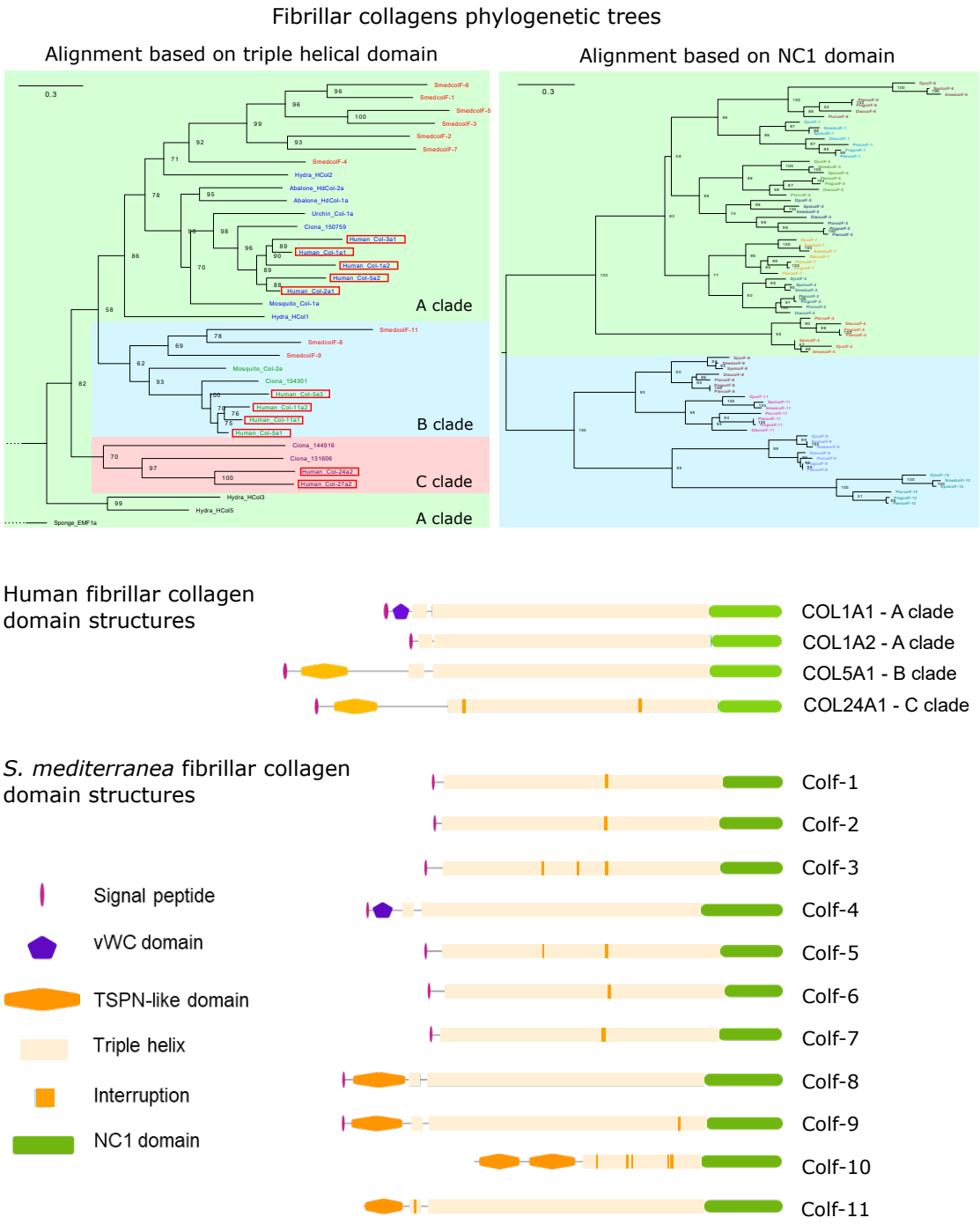

Figure S2. Fibrillar collagens phylogenetics and peptide domains.
Top panels: Phylogenetic trees of fibrillar collagen protein sequences constructed using maximum likelihood. The numbers represent bootstrap values generated from 10,000 replicates. The scale bar represents 0.3 substitutions per amino acid site. Fibrillar collagens are clustered into A, B and C clades (green, blue and pink box, respectively). “Smedcolf”: S. mediterranea-colf chains; “Djcolf”: *Dugesia japonica*-colf chains. Red hollow boxes highlighted human fibrillar collagen sequences. Left: Tree built using multiple sequence alignment based on triple helical domain. Right: Tree built using multiple sequence alignment based on NC1 domain. Bottom panel: fibrillar collagen peptide domains. The general domains are similar between human and planarian homologs, except most planarian homologs have more chain interruptions. Smedcolf-10 has a unique short triple helical domain with highest number of chain interruptions, and is the only chain with two TSPN-like domains in N-terminal.

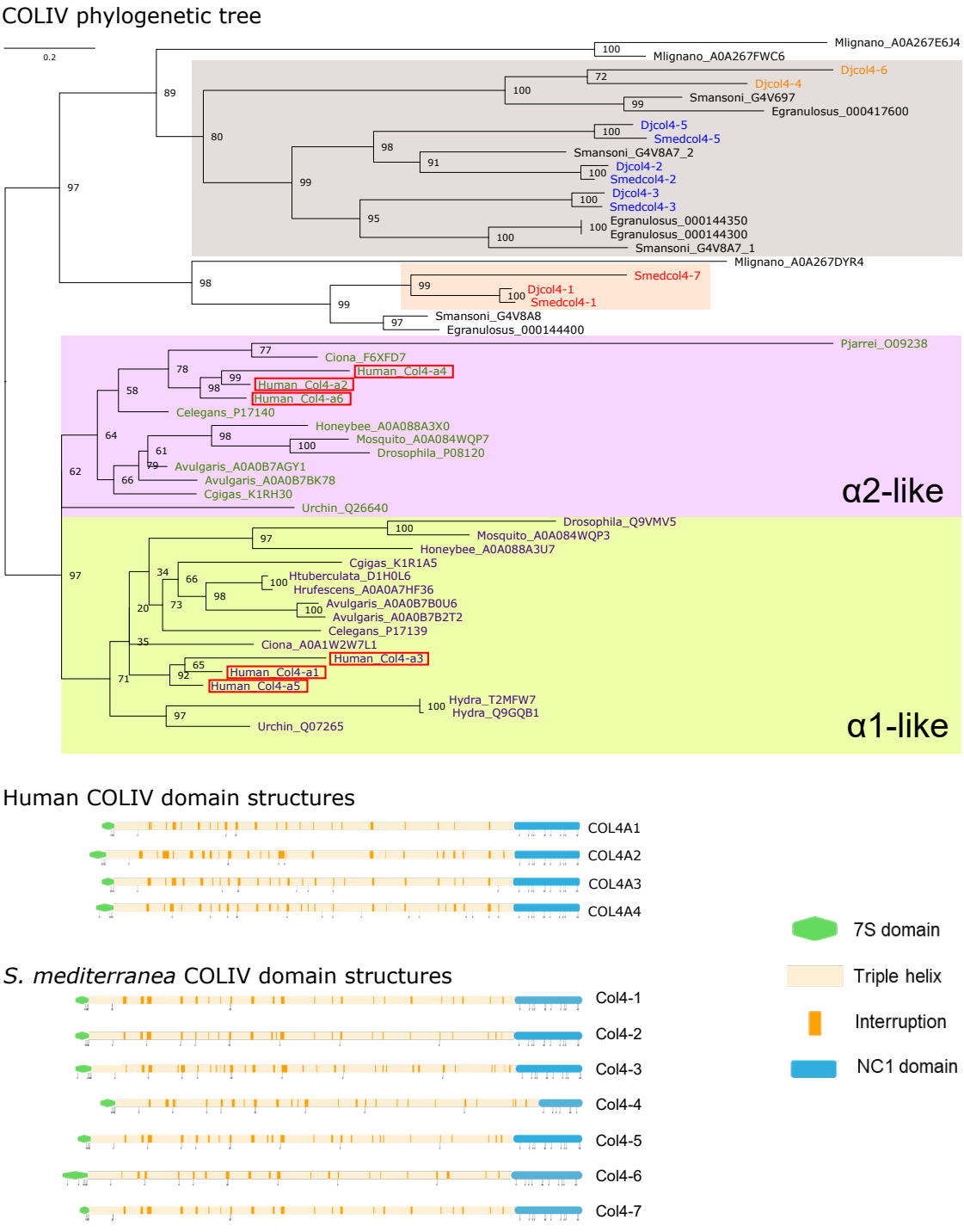

Figure S3. COLIV phylogenetics and peptide domains.
Top panel: Phylogenetic tree of COLIV protein sequences constructed using maximum likelihood using the multiple sequence alignment of the NC1 domain. The numbers represent bootstrap values generated from 10,000 replicates. The scale bar represents 0.2 substitutions per amino acid site. COLIV in human, *C. elegans*, hydra and insect species can be grouped into α1-like (yellow) and α2-like (violet) subclusters. In contrast, flatworm COLIV chains form a separate clusters (orange and grey); the grey cluster can be further divided into two sub-clusters (light grey), annotated by blue and orange characters. Bottom panel: All planarian COLIV peptide domains are similar to human homologs.

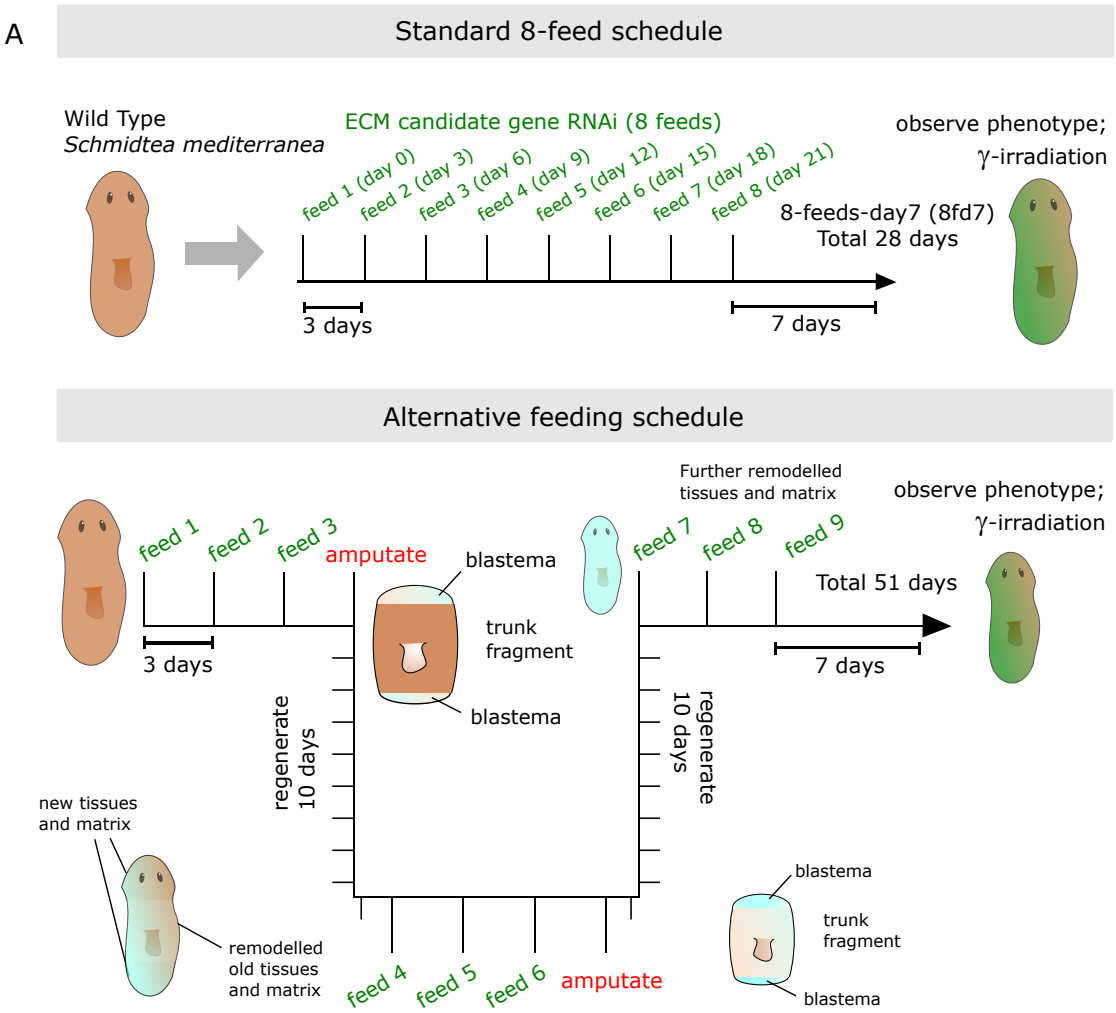

B

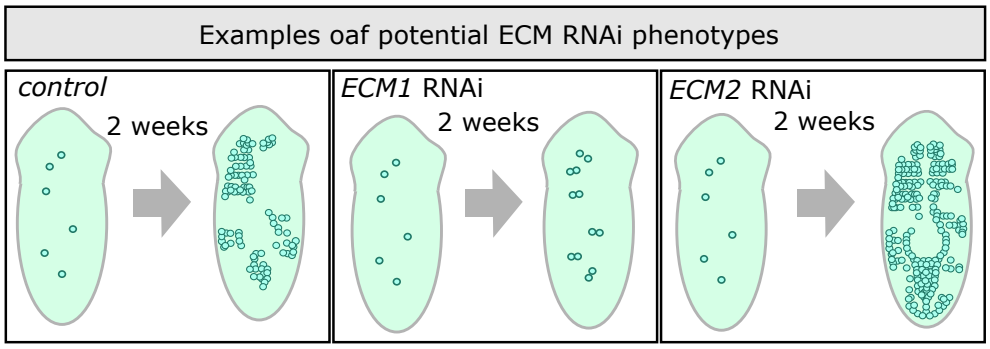

Figure S4. RNAi feeding schedules in ECM screening.
(*A*) RNAi Screening is first done by the Standard 8-feed schedule (top panel). Genes without any observable neoblast repopulation phenotypes after the primary schedule will be re -screened using the Alternative feeding schedule (bottom panel) which underwent additional rounds of feeding and amputations to facilitate further ECM turnover in RNAi animals. (B) Schematic diagrams outlining the potential outcomes that can be obtained in the neoblast repopulation assay in reference to *control(RNAi)* with lower neoblast density for *ECM1(RNAi)* and higher neoblast density for *ECM2(RNAi)*.

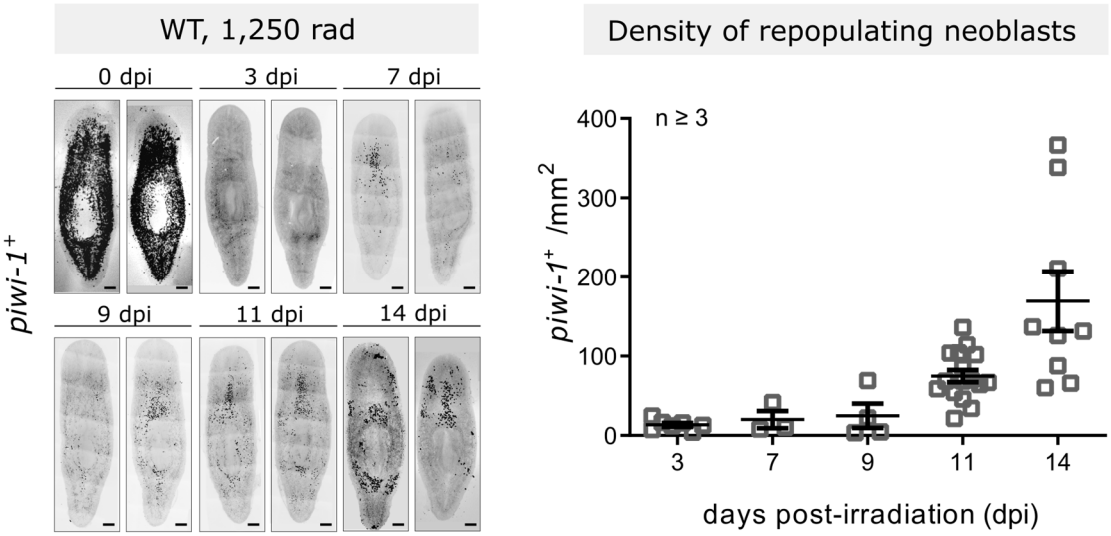

Figure S5. Neoblast repopulation in wild type worms.
A demonstration of neoblast repopulation during the first 14 days. Wild type planarians received a dose of 1,250 rad of γ-irradiation, which eliminated most neoblasts from 0-3 days post-γ-irradiation (dpi). Repopulation is observed from 3-14 dpi. Left: Neoblast population (*piwi-1*$^+$) in each time point is stained by FISH and observed by spinning disc confocal under tiled Z-projections (2 representative images per time point). Scale bar = 100 μm. Right: Density of neoblasts in each time point is quantified. Number of animals tested is indicated by the number of data points in each group. Mean ± s.e.m is presented.

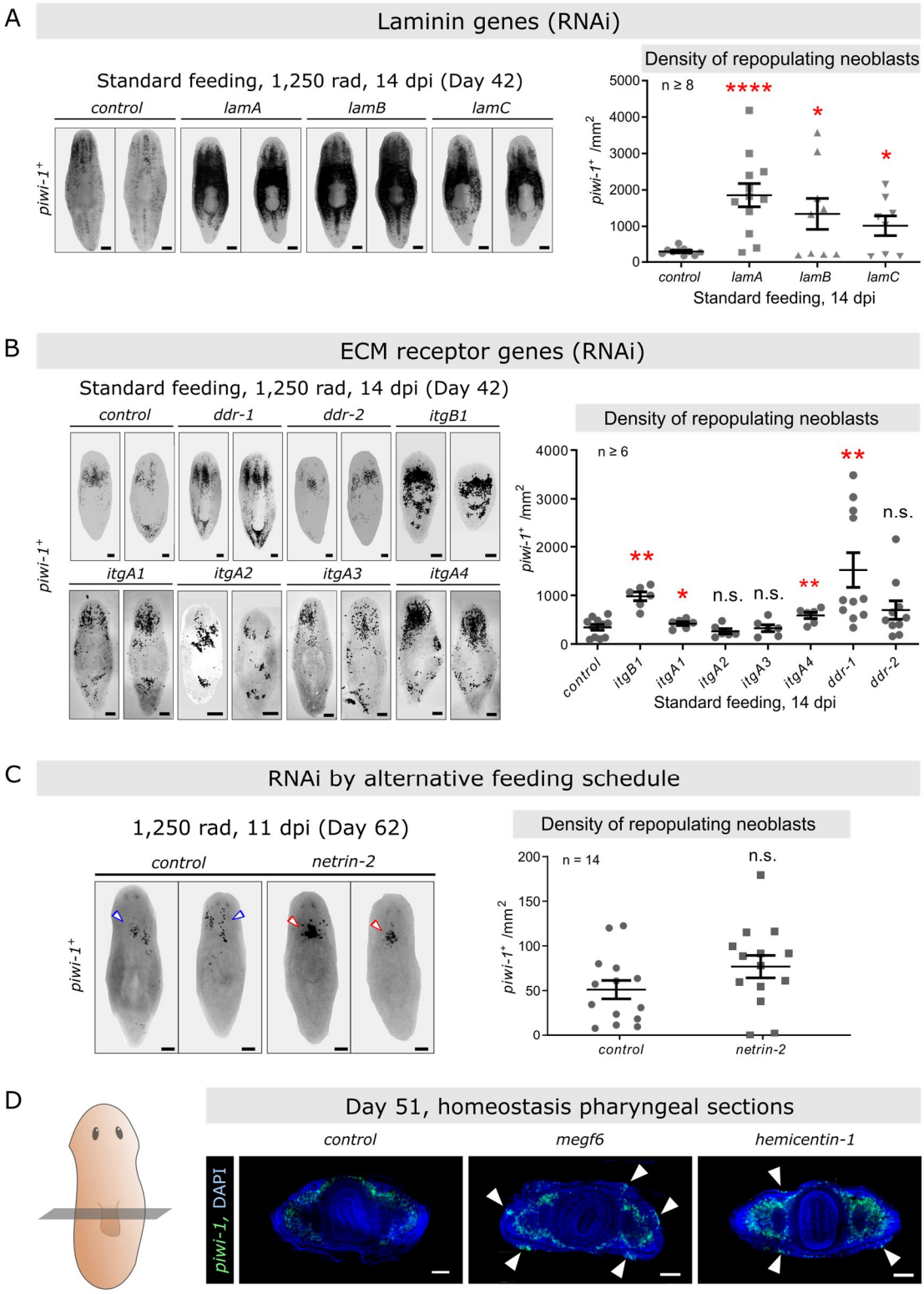

Figure S6. Neoblast defects in *laminin(RNAi)*, *ddr(RNAi)* and *integrin(RNAi)* worms.
(*A*) Representative confocal-images of neoblast (*piwi-1*$^+$) FISH stains and quantification of their densities in worms with *laminin(RNAi)* (*lamA, lamB* and *lamC*) under standard feeding schedule (8fd7), followed by 1,250 rad γ-irradiation and 14 days of repopulation. (*B*) Representative confocal-images of neoblast (*piwi-1*$^+$) FISH stains and quantification of their densities in worms with *ECM receptor(RNAi)* (*itgB1, itgA1, itgA2, itgA3, itgA5, ddr-1* and *ddr-2*) under standard feeding schedule (8fd7), followed by 1,250 rad γ-irradiation and 14 days of repopulation. (*C* and *D*) Neoblast phenotypes obtained by Alternative feeding schedule. (*C*) *netrin-2(RNAi)* result in no significant repopulation rate (Right), but clumping of repopulating neoblasts in anterior region (left, red arrowhead) compared to *control(RNAi)* (blue arrowhead) at 11 dpi. (*D*) *hemicentin-1(RNAi)* and *megf6(RNAi)* resulted in ectopic neoblast emergence in epidermal region (arrowheads). Representative images showed mid-body transverse sections. For all images, scale bar = 100 μm. For all graphs, number of animals tested is indicated by the number of data points in each group. Mean ± s.e.m is presented, and statistical significance was assessed using two-tailed unpaired Student *t* tests. *p<0.05; **p<0.01; ***p<0.001; ****p<0.0001. Confocal images are shown as tiled Z-projection (*A-C*) or single Z-plane (*D*).

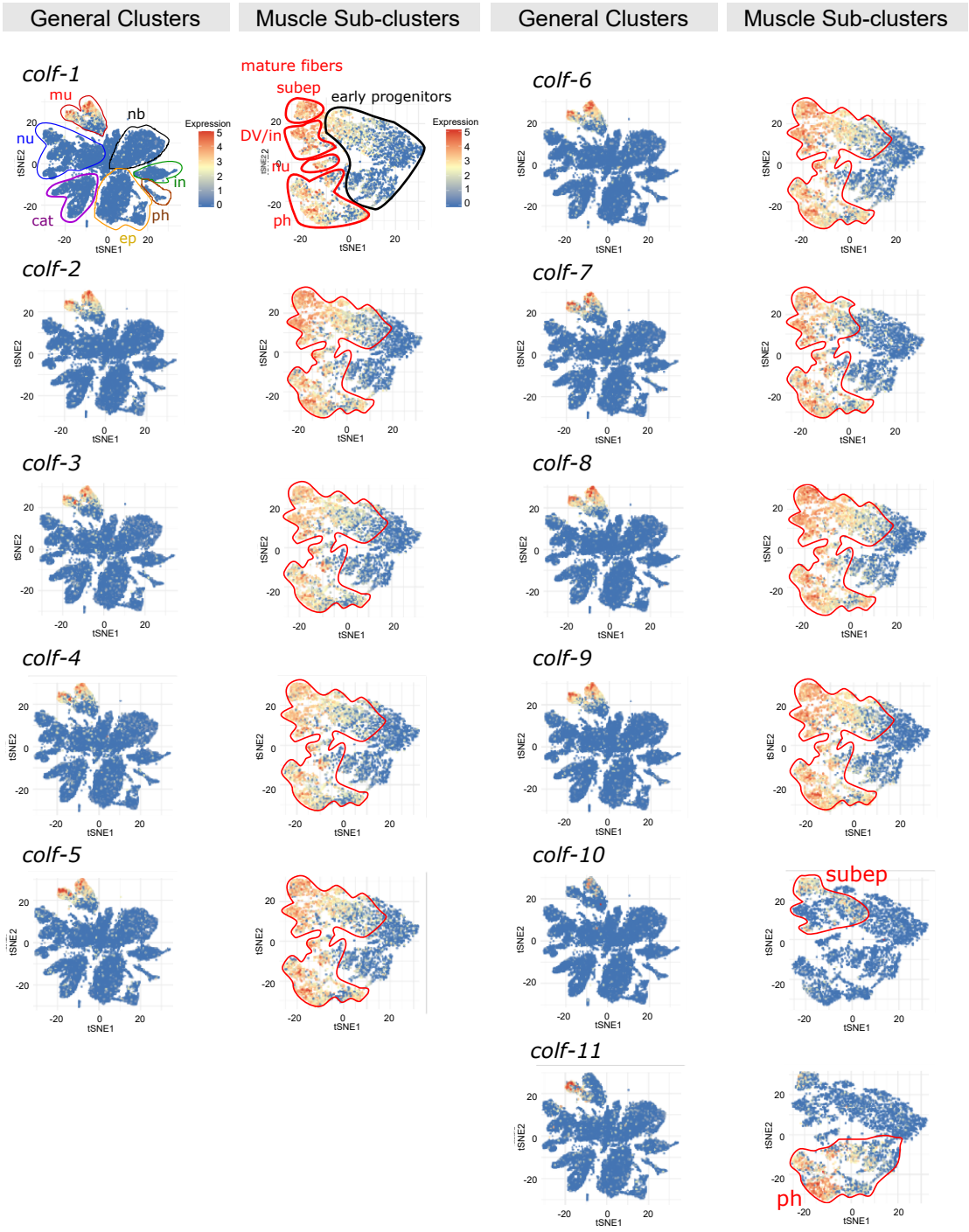

Figure S7. Expression of fibrillar and short chain collagens shown by scRNAseq tSNE plots.
Expressions of *colf-1 – 11* in Main clusters and Muscle sub-clusters. Red lines highlights collagen-expressing clusters. Heat maps of tSNE plots are plotted by ln(UMI -per-10,000 +1). “nb” neoblast, “plu” pluripotent, “ep” epidermis, “in” intestine, “ph” pharynx, “mu” muscle, “nu” neuron., “pn” protonephridia, “cat” cathepsin+, “DV” dorsal-ventral, “subepi” subepidermal.

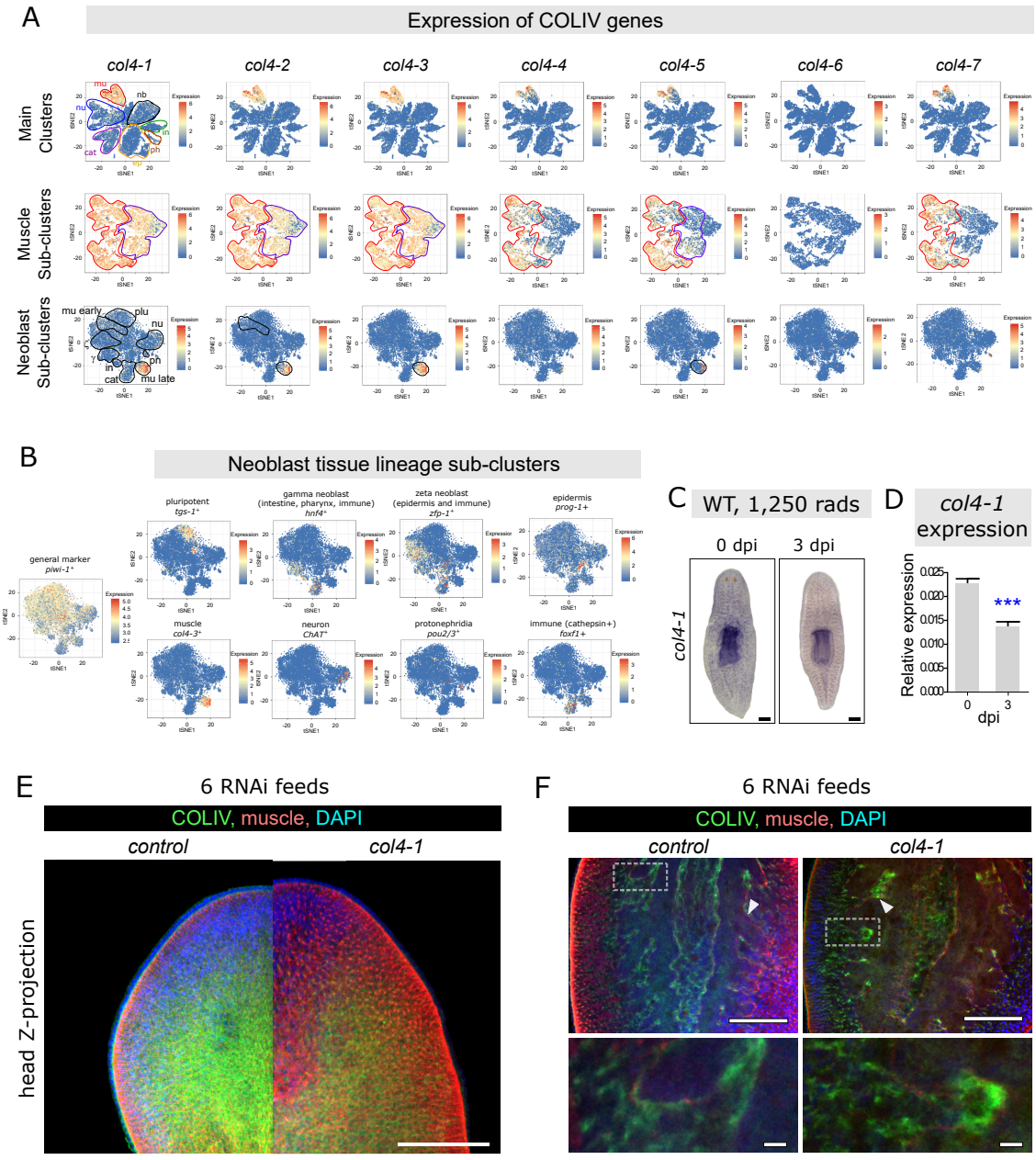

Figure S8. Expression of COLIV.
(*A*) scRNAseq tSNE plots of COLIV genes, shown in main clusters (top), muscle sub-clusters (middle) and neoblast sub-clusters (bottom). In muscle sub-clusters, red lines enclosed clusters of mature muscle cells expressed by the COLIV genes; purple lines enclosed early progenitors. For neoblast sub-clusters, black lines enclosed neoblast types that express the corresponding COLIV gene. "plu" pluripotent, "γ" gamma, "ζ" zeta, "mu" muscle, "in" intestine, "nu" neuron., "pn" protonephridia, "cat" cathepsin+. (B) Annotation of different neoblast sub-clusters with corresponding marker genes. Left panel: general neoblast marker *piwi-1* is expressed by most neoblast cells. Right panels: marker genes specifically expressed by different neoblast sub-populations. (C and D) Expression change of COLIV gene *col4-1* before and after selective neoblast removal (3 dpi after 1,250 rad γ-irradiation) is shown by ISH (C) and qRT-PCR (gene expression relative to housekeeping gene gapdh) (D). Each group is conducted with biological triplicate and experimental triplicates. Mean ± s.e.m is presented, and statistical significance was assessed using two-tailed unpaired Student *t* tests. ***$p<0.001$. (*E*) Confocal maximum intensity Z-projection of the head region in *control(RNAi)* and *col4-1(RNAi)* worms after 6 RNAi feeds (Day 22), COLIV (αCOLIV) and muscle (α6G10) stains. (*F*) Single Z-plane dorsal view of the parenchymal region in RNAi worms. Lower panels are enlarged gut-parenchymal region, where dense COLIV patches are found only in *col4-1(RNAi)* worms. Scale bars in *C, E* and *F*: upper panels = 100 μm; *F* lower panels = 10 μm.

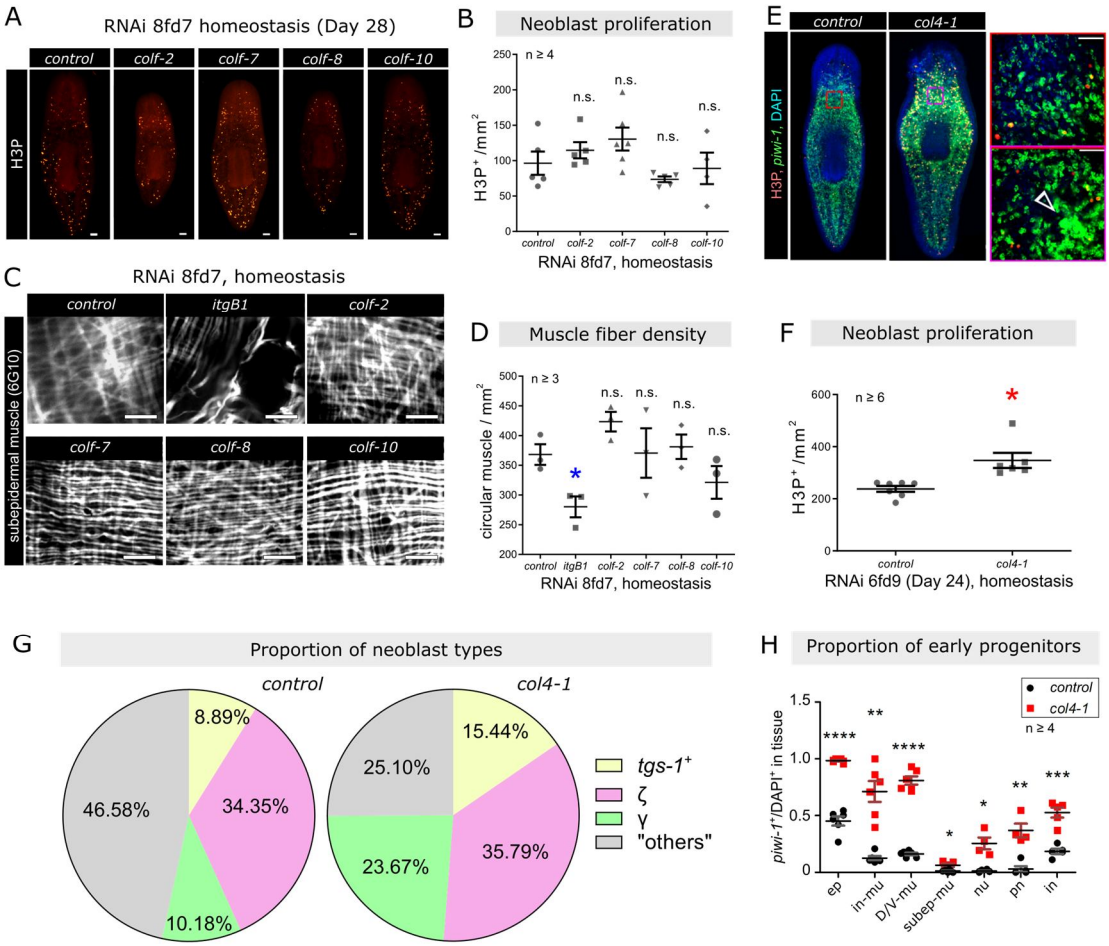

Figure S9. Phenotypes of fibrillar, short chain and type IV collagen RNAi under non-γ-irradiated condition.
(*A*) Representative images of H3P stains in *control(RNAi)* and *fibrillar/short chain collagen(RNAi)* worms. Scale bar = 100 μm. (*B*) Quantification of H3P⁺ cell density. (*C*) Confocal multiple Z-plane-images showing *fibrillar/short chain collagen(RNAi)* worms have intact musculature as seen in *control(RNAi)* worms, as opposed to *itgB1(RNAi)* muscles with disorganized fibers. Scale bar = 10 μm. (*D*) Quantification of Muscle fiber density. (*E*) Confocal tiled Z-projection images of *piwi-1* and H3P stains in *control(RNAi)* and *col4-1(RNAi)* worms. Scale bar = 100 μm. Right small panels are zoomed-in images of anterior parenchymal regions. Hollow arrowhead highlights dense neoblast clusters. Scale bar = 50 μm. (*F*) Quantifications of H3P⁺ cell density. (*G*) The relative proportions of *tgs-1*⁺, ζ and γ neoblasts within neoblast pool. (*H*) Quantification of the proportion of *piwi-1*+ cells within early epidermal progenitors (ep) (*zfp-1*⁺), protonephridia (pn) (*cavII*⁺), neuron (nu) (*ChAT*⁺), intestine (in) (*hnf4*⁺), D/V muscles (D/V-mu), gut muscles (in-mu) and subepidermal muscles (subep-mu) (*col4-2*⁺).For graphs in *B, D, F* and *H*, number of animals tested is indicated by the number of data points in each group. Mean ± s.e.m is presented, and statistical significance was assessed using two-tailed unpaired Student *t* tests. **p*<0.05; ***p*<0.01; ****p*<0.001; *****p*<0.0001.

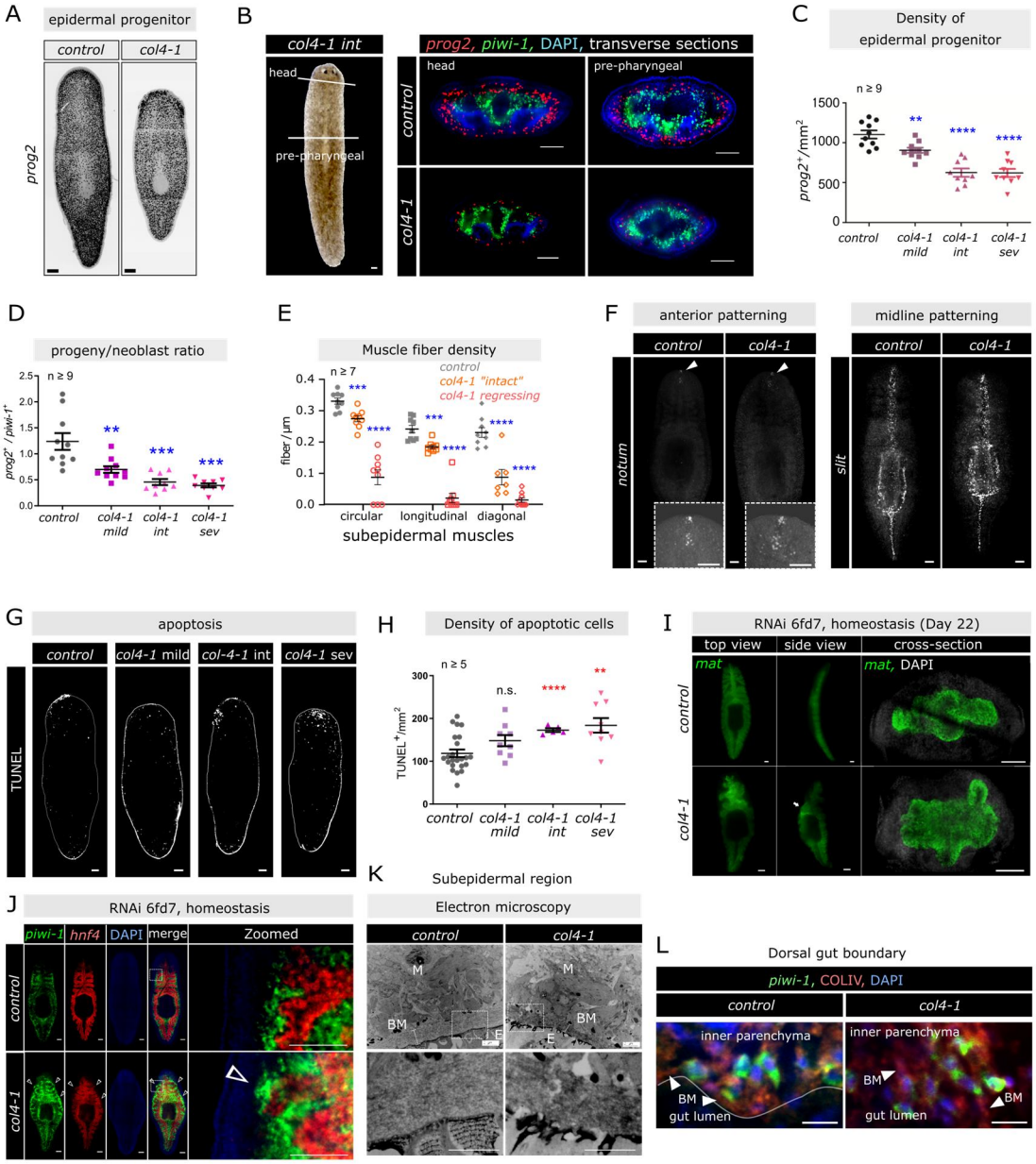

Figure S10. Tissue loss and disorganization in late stage *col4-1(RNAi)* worms.
(*A*) Tiled Z-projection confocal images of whole worm-epidermal progenies *prog2*⁺ FISH stain of *control(RNAi)* and *col4-1(RNAi)* intermediate phenotype (Imaged taken by spinning disc confocal microscopy). (B) Left panel: demonstration of locations where transverse sections are taken for FISH analysis, in *control(RNAi)* and *col4-1(RNAi)* worms. These include head (post-eyespot and non-regressing zone) and pre-pharyngeal region (immediately in front of pharynx). Right panels: Single Z-plane confocal images of neoblasts (*piwi-1*⁺), early epidermal progenies (*prog2*⁺) and cell nuclei (DAPI) in anterior (intact region) transverse sections of *control(RNAi)* and intermediate *col4-1(RNAi)* worms. Scale bar = 100 µm. (*C*) Quantifications of *prog2*⁺ cell densities along different regression severities (int: intermediate; sev: severe). (*D*) Quantifications of epidermal progenitor-to-neoblast ratio in head transverse sections. (*E*) Density quantification of circular, longitudinal and diagonal muscle fibers at regressing and "intact" regions of the heads, respectively. (*F*) Expression of patterning control genes *notum* and *slit* in *control(RNAi)* and intermediate *col4-1(RNAi)* worms. (*G*) Apoptosis of *control(RNAi)* and *col4-1(RNAi)* worms from mild to severe phenotypes, stained with TUNEL⁺ cells. (*H*) Quantification of apoptotic cell density. Number of animals tested is indicated by the number of data points in each group. Mean ± s.e.m is presented, and statistical significance was assessed using two-tailed unpaired Student *t* tests. ***p*<0.01; *****p*<0.0001. (*I*) Gut disorganization in *col4-1(RNAi)* 6 feeds is visualized by ISH of gut marker *mat*. Top view (coronal), side view (sagittal) and neck cross-sections (transverse, counterstained with DAPI). Regions of gut outgrowth or disorganization is indicated by a white arrow. (*J*) dFISH of gut (*hnf4*⁺) and neoblast (*piwi-1*⁺). Right panels are enlarged from white boxes in "merged" images. Arrowheads indicate co-localizations of dense *piwi-1*⁺ clusters and disorganized gut branches. Scale bar in *A-J* = 100 µm. (*K*) Representative electron microscopy images of intact anterior lateral region subepidermal BM and muscle fibers "M" in *control(RNAi)* and intermediate *col4-1(RNAi)* worms, 8fd7. White boxes highlight regions of BM that is enlarged in lower panels. Scale bar = 2 µm. (*L*) Neoblast (*piwi-1*⁺) and BM (COLIV⁺) localizations at gut-inner parenchyma boundary is visualized in *control(RNAi)* and intermediate *col4-1(RNAi)* worms. White line in *control(RNAi)* image highlights a clear boundary between the two tissue compartments. Scale bar = 10 µm. Confocal images are shown as tiled Z-projection (*A, F, G, I* (coronal, sagittal)) or single Z-plane (*B, I* (transverse), *J, L*).

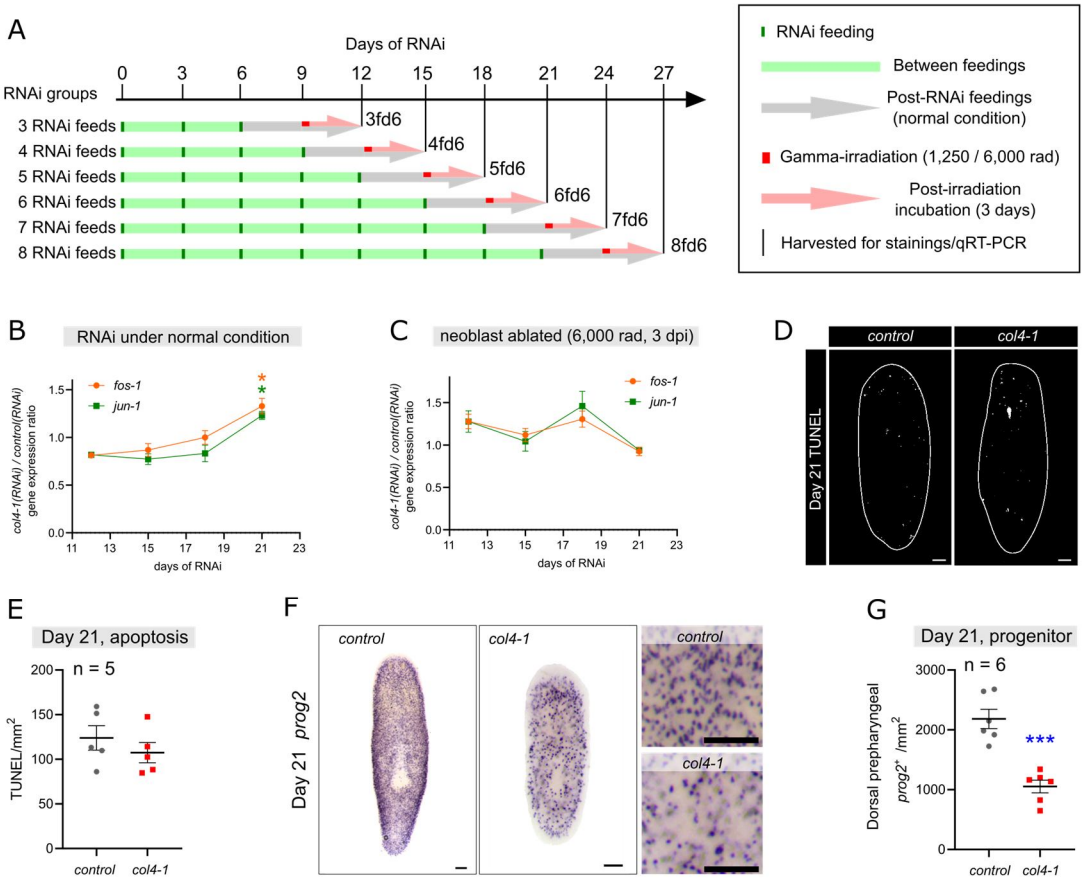

Figure S11. Time point comparison of tissue wounding and neoblast phenotypes in *col4-1(RNAi)* worms
(*A*) Schematic diagram of experimental setups. *control/col4-1* RNAi worms were separated into 6 groups with 3 – 8 doses of RNAi feeds, respectively. Each round of feeding was 3 days apart. After the last feed, worms were maintained without feeding for 3 more days before proceeding to lethal (6,000 rad), sublethal (1,250 rad) or no γ-irradiation, and incubated for 3 more days before harvesting. 3fd6: 3-feeds-day6, 4fd6: 4-feeds-day6, 5fd6: 5-feeds-day6, 6fd6: 6-feeds-day6, 7fd6: 7-feeds-day6, 8fd6: 8-feeds-day6. (*B* and *C*) Fold change of wounding genes *fos-1* and *jun-1* in *col4-1(RNAi)* worms compared to *control(RNAi)* worms, from 12 days of RNAi (3fd6) to 21 days of RNAi (6fd6), under homeostatic (*B*) and lethally γ-irradiated 3 dpi (*C*) conditions, respectively. In this qRT-PCR, each group is done with biological triplicate and experimental triplicate. Data represent the mean ± s.e.m and statistical significance was assessed using two-tailed unpaired Student *t* tests. **p*<0.05. (*D* and *E*) Apoptotic cell density determined by TUNEL, in 21 days of RNAi worms. Confocal (tiled Z-projected) images in *C* and quantifications in *E*. *F* Representative images of *prog2* colorimetric-ISH stain in 21 days of RNAi worms, *prog2*+ cell density in dorsal prepharyngeal region (between eyespot and pharynx) is quantified in *G*. In each group mean ± s.e.m is presented, and statistical significance was assessed using two-tailed unpaired Student *t* tests. n.s. not significant, ***p*<0.01. For all images, scale bar = 100 μm.

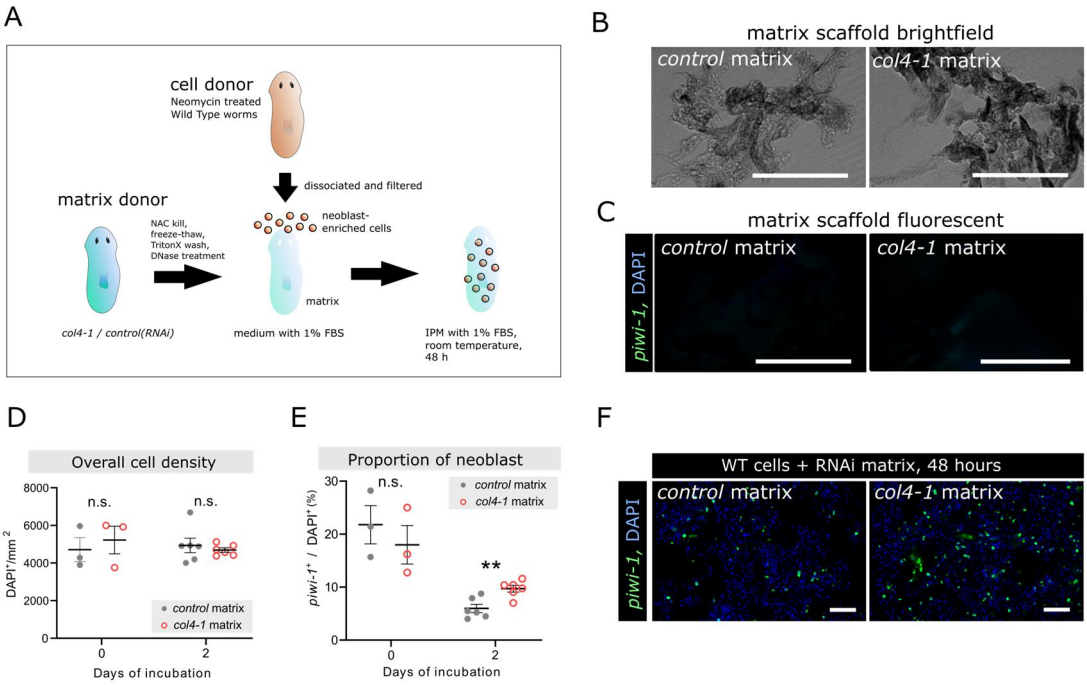

Figure S12. *in vitro* neoblast culturing in *col4-1(RNAi)* ECM scaffold
(*A*) Schematic diagram showing how matrix scaffolds are prepared, how cells are isolated, and how the co-incubation is done. (*B* and *C*) Cell-free matrix scaffold (no cell seeded) were shown under brightfield (*B*) and FISH with *piwi-1* and DAPI stain (confocal single *Z*-plane) (*C*), confirming no viable cells exist. (*D*) Wild type cell density and (*E*) the percentage of neoblasts (*piwi-1*$^{+}$/DAPI^{+}) are determined in tissue culture on *control(RNAi)* and *col4-1(RNAi)* matrix scaffold, after 0 and 2 days of incubations, respectively. Number of replicates tested is indicated by the number of data points in each group. In each group mean ± s.e.m is presented, and statistical significance was assessed using two-tailed unpaired Student *t* tests. n.s. not significant, $^{**}p<0.01$. (*F*) Confocal images of tissue culture on *control(RNAi)* and *col4-1(RNAi)* matrix scaffold after 2 days of incubation. For all images, scale bar = 100 μm.

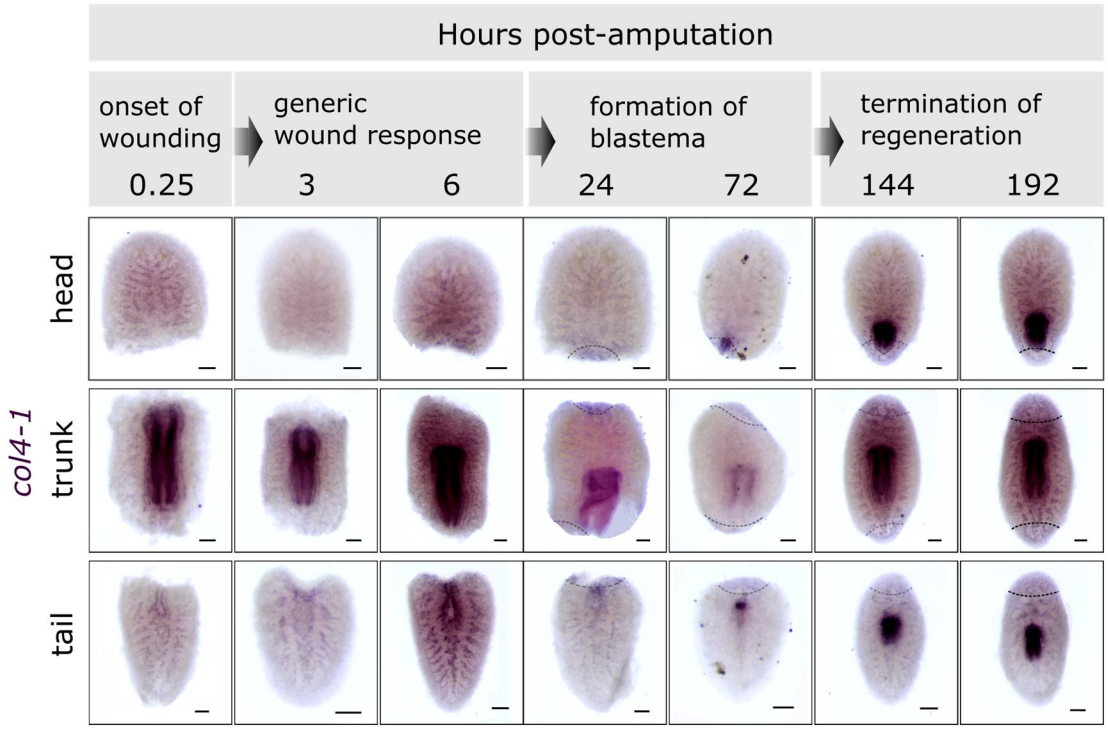

Figure S13. Expression of *col4-1* across regeneration
Expression of *col4-1* by colorimetric-ISH in WT worms from amputation to full regeneration over a period of 192 hours (8 days). The boundary between the blastemal and old tissue is indicated by dotted black lines. Scale bar = 100 μm.

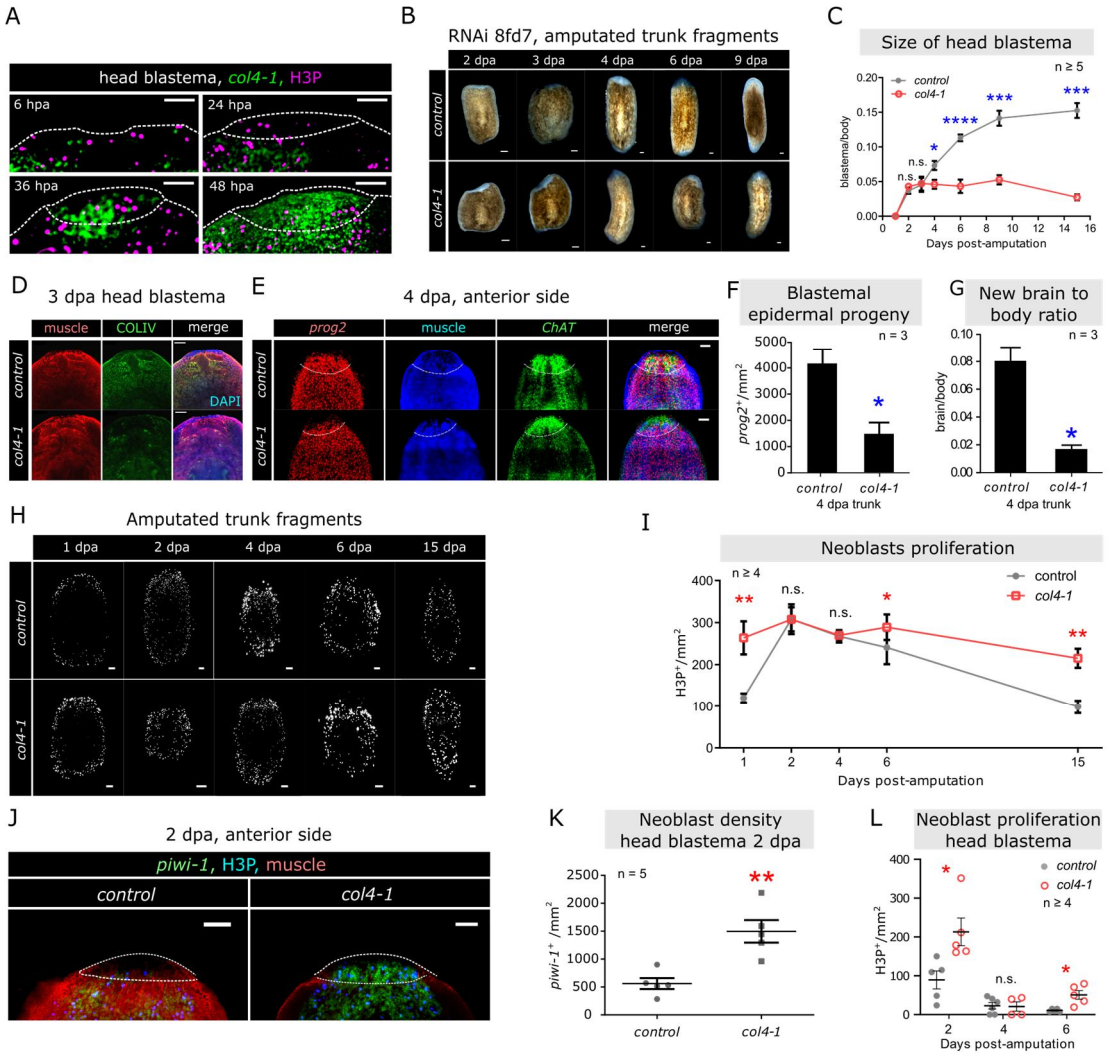

Figure S14. Impaired tissue regeneration in *col4-1(RNAi)* worms
(*A*) Representative images showing increasing *col4-1* expression in the blastema region correlates with reducing neoblast proliferation from 6 – 48 hpa. White dotted lines highlighted edge of animals. (*B-L*) *control(RNAi)* and *col4-1(RNAi)* worms amputated at 7 days after 8-RNAi feeds (8fd7) at regions anterior and posterior of the pharynx, these trunk fragments are allowed to fully regenerate over 15 days. (*B*) Growth of blastema (white tissue at top and bottom of fragments) from 2 – 9 dpa. (*C*) Quantification of the anterior blastemal size to whole body size ratio. (*D*) αCOLIV and α6G10 (muscle) stains. (*E*) Epidermal (*prog2*$^+$), muscle (6G10$^+$) and brain (*ChAT*$^+$) cells. Dotted lines: blastema/old tissue boundary. (*F*) Quantifications of blastemal epidermal progeny densities. (*G*) Quantification of the new brain/whole body area ratio. (*H*) Proliferating neoblasts (H3P$^+$) in trunk fragments. (*I*) Quantification of H3P$^+$ density from 1 – 15 dpa. (*J*) Assessment of proliferating neoblasts (H3P$^+$/*piwi-1*$^+$) in blastemal region of *col4-1(RNAi)* worms. (*K*) Quantifications of neoblasts (*piwi-1*$^+$), and (*L*) proliferation (H3P$^+$) densities. For regeneration experiments, number of animals tested is indicated by the number of data points in each group. Mean ± s.e.m is presented, and statistical significance was assessed using two-tailed unpaired Student *t* tests. **p*<0.05; ***p*<0.01; ****p*<0.001; *****p*<0.0001. All scale bars = 100 μm. *A, D, E, H* and *J* are tiled Z-projected confocal images.

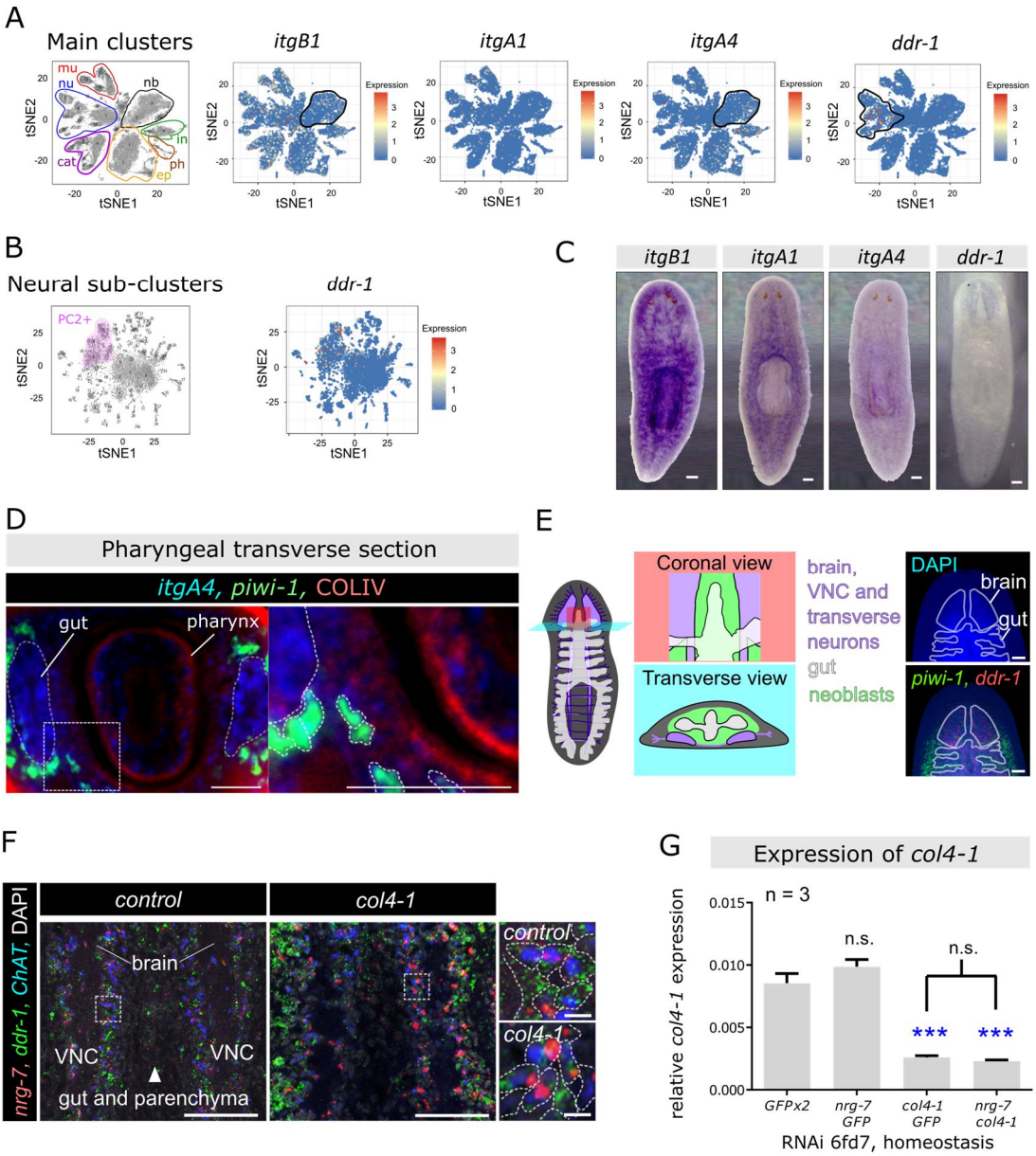

Figure S15. ECM receptors integrin and DDR RNAi resulted in increased rate of neoblast repopulation
(*A* and *B*) Expressions of *itgB1, itgA1, itgA2* and *ddr-1*, determined by scRNAseq tSNE plots, in main clusters (*A*) and neural sub-cluster for *ddr-1*, where PC2⁺ neurons are highlighted (*B*). Circles in *itgB1* and *itgA2* plots indicate expression of these genes in neoblast cluster; circle in *ddr-1* plot indicates expression in neural cluster. (*C*) Colorimetric-ISH of each ECM receptor's whole-body expression. (*D*) Triple FISH/IF of *itgA4* with neoblasts (*piwi-1*⁺) and COLIV (mid-body transverse section). (*E*) Schematic diagram showing the proximity of neoblasts (in parenchyma), neurons and gut, in dorsal and transverse views. Right panels: confocal visualization of brain and gut structures by DAPI is demonstrated, together with *piwi-1* FISH. (*F*) FISH of *nrg-7, ddr-1, ChAT* and DAPI in *control(RNAi)* and *col4-1(RNAi)* animals at 18 days of RNAi (6fd3), under the same imaging condition (laser power and exposure time) compared *nrg-7* expression level in *ddr-1*⁺/*ChAT*⁺ neurons. (*G*) Expression of *col4-1* in double RNAi groups (6fd7, non-γ-irradiated) by qRT-PCR. Gene expression levels are normalized by house-keeping gene *gapdh*. Each group is done with biological triplicate (each consisted of cDNA pooled from 3 worms) and experimental triplicate. Data represent the mean ± s.e.m and statistical significance was assessed using two-tailed unpaired Student *t* tests. ***$p<0.001$, n.s. not significant. *D, E* and *F* are single *Z*-plane confocal images. Scale bars: *F* small panels = 10 μm; all others = 100 μm.

Original images of figure panels where the background was removed for presentation in the main figures

Fig. 1

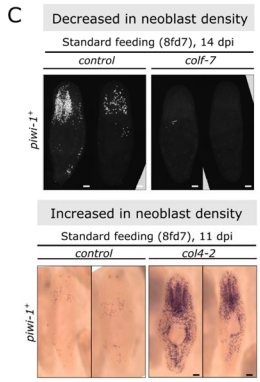

Fig. 2

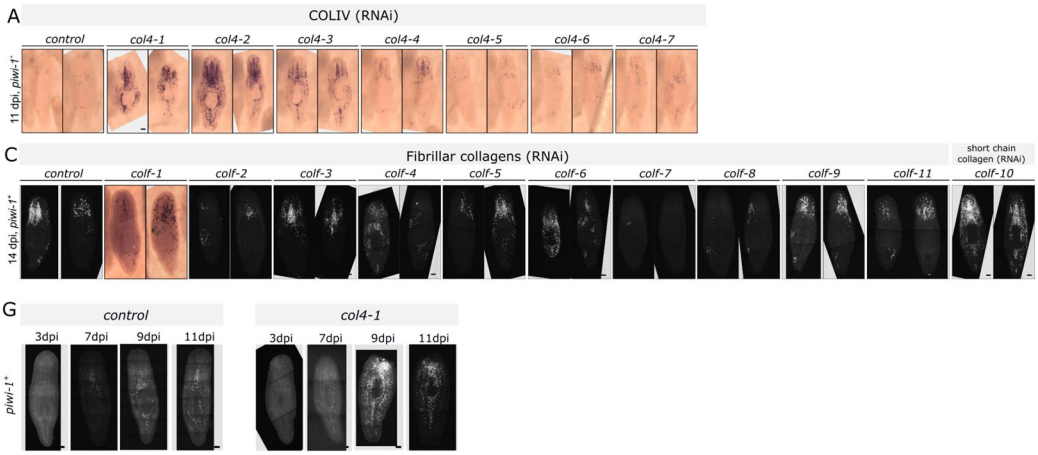

Fig. 3

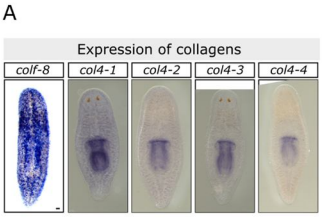

Fig. 5